ELSEVIER

Nuclear Engineering and Design 175 (1997) 37–48

Nuclear Engineering and Design

Investigation of flow structures in vertical slug flow

M. Kawaji *, J.M. DeJesus, G. Tudose

Department of Chemical Engineering and Applied Chemistry, University of Toronto, Toronto, Ont., Canada M5S 3E5, USA

Received 14 January 1997; accepted 12 June 1997

Abstract

The flow structure of gas–liquid slug flow in a vertical tube has been investigated experimentally and numerically. A photochromic dye activation method was used to obtain two-dimensional liquid velocity profiles around a Taylor Bubble rising in stagnant kerosene in a vertical 25.6 mm I.D. pipe. A numerical simulation of the flow was conducted using a Volume-of-Fluid approach to predict both the shape of the Taylor Bubble and the velocity profiles in the liquid phase. In order to test the hypothesis that a trailing bubble can accelerate, catch up and coalesce with a leading bubble because of lateral motion and reduced drag force, a second experiment was performed using a solid Taylor Bubble placed in a steady downward flow of liquid. The measured drag force showed significant reduction as the bubble was moved from the tube axis towards the wall, giving support to the hypothesis. © 1997 Elsevier Science S.A.

1. Introduction

Gas–liquid slug flow is widely encountered in many industries and equipment such as geothermal power, chemical and nuclear reactors, oil and gas wells, and in heat exchangers such as steam generators and kettle reboilers. Although slug flow is seemingly a well-ordered flow, it is highly complex with an unsteady nature, showing wide distributions in gas and liquid slug lengths. It has also been extensively studied in the past, however, certain aspects of flow still remain poorly understood, due to the lack of detailed data on the flow structure.

For example, the question of how and why a trailing Taylor Bubble accelerates and coalesces with a preceding Taylor Bubble has not been answered. This requires understanding of the hydrodynamics of the liquid surrounding a Taylor Bubble, since the global flow characteristics such as rise velocity and void fraction are highly dependent on the nature of liquid flow. To this end, we have applied the photochromic dye activation method (PDA) to obtain detailed hydrodynamic data on the flow structure of the liquid phase, conducted numerical simulations of the flow using a Volume-of-Fluid (VOF) method, and are now examining experimentally the drag force on a solid Taylor Bubble at different radial positions in order to determine the mechanism of Taylor Bubble acceleration and coalescence in continuous slug flow in a vertical tube.

* Corresponding author. Fax: +1 416 9788605; e-mail: kawaji@ecf.toronto.edu

PII S0029-5493(97)00160-X

1.1. Previous work

Slug flow in vertical tubes has been investigated since the early 1940s. Dumitrescu (1943) was among the first to study a single Taylor Bubble rising in a stagnant liquid in a tube and attempted to model this flow based on a potential flow theory. He theoretically derived a Taylor Bubble shape for air-water systems that agrees very well with experimental observations of others such as Mao and Dukler (1989). Davies and Taylor (1950) used a similar approach, in part to derive the rise velocity of gas slugs. Presently, the Taylor Bubble rise velocity in a quiescent liquid inside a closed pipe of diameter D is given by,

$$U_{TB} = 0.35\sqrt{gD} \quad (1)$$

Many other researchers have undertaken further investigations of slug flow: Moissis and Griffith (1962), Nicklin et al. (1962), Street and Tek (1965), Akagawa et al. (1970), Collins et al. (1978), Fukano et al. (1980), Bendiksen (1985), Nickens and Yannitell (1987), Reinelt (1987), Couët and Strumolo (1987), among others. More recently, Mao and Dukler (1991) and Tomiyama et al. (1993) have attempted to model vertical slug flow numerically by solving the Navier-Stokes equations without making a priori assumptions about the shape of the gas slug. Shemer and Barnea (1987) used a hydrogen bubble technique to study the liquid flow field in the wake of a Taylor Bubble. DeJesus et al. (1995) presented the first measurements of the velocity profiles in the liquid phase surrounding a single Taylor Bubble rising through a stagnant liquid in a vertical tube. To date, however, there has not been any comparison of velocity fields between measurements and numerical model predictions.

There are some aspects of the liquid film flow around the Taylor Bubble which need to be better understood in order to develop more accurate global models of slug flow. Dumitrescu (1943) assumed the film flow to be inviscid. Brown (1965) assumed the film was fully developed and the flow was laminar. Fernandes et al. (1983) also used this relation, but allowed for turbulent flow conditions to obtain a hydrodynamic model for slug flow. Many models assume that the velocity profile in the falling film is fully developed and that the film is of constant thickness. According to Fabre and Liné (1992), assuming a fully developed velocity profile underestimates the mean film thickness. This weakness is particularly important for short bubbles which are a few diameters in length.

Another important question that remains to be answered is the mechanism of Taylor Bubble acceleration and coalescence. When two Taylor Bubbles flow upward separated by a certain distance, the trailing bubble may (or may not) accelerate, catch up and coalesce with the leading Taylor Bubble depending on the separation distance. Moissis and Griffith (1962) developed an empirical correlation for the accelerating rise velocity of a Taylor Bubble as a function of the decreasing distance behind a leading Taylor Bubble, however, the exact mechanism for Taylor Bubble acceleration is still unclear. Dukler et al. (1985) and Shemer and Barnea (1987) hypothesized that there is a minimum stable liquid slug length beyond which the Taylor Bubbles would rise at the same velocity and would not coalesce. Dukler et al. (1985) formulated a criterion for the minimum stable liquid slug length (or the minimum separation distance between two successive Taylor Bubbles) based on the growth of momentum boundary layers in the liquid behind the wake of a preceding bubble. However, their hypothesis has not been verified experimentally.

2. Experimental work

2.1. Velocity field measurements

DeJesus et al. (1995) used a Photochromic Dye Activation (PDA) method to obtain the velocity profiles in the liquid flowing past a Taylor Bubble rising through stagnant kerosene in a vertical tube as shown in Fig. 1. The test section was a 3.03 m long, 25.6 mm I.D. Pyrex pipe. The kerosene (at 20°C, $\rho = 755$ kg m^{-3}, $\mu = 1.43$ mPa s^{-1}, and $\sigma = 21.4$ dynes cm^{-1}) had a small quantity of photochromic dye (TNSB) dissolved in it at a concentration of 0.01%. The details of the measurement technique have been given by Kawaji et

al. (1993). To minimize entrainment of small bubbles in the wake of the Taylor Bubble, air was injected into a 3.00 m long, 25.6 mm I.D. flexible developing section consisting of a horizontal section followed by a long sweeping, gradually inclined bend connected to the test section.

The dye trace sequences were recorded using a high speed CCD video camera (Photron 11B) which captured the images at a rate of 1297 or 1488 frames s^{-1} with a shutter speed of 5 kHz. Images were analyzed on a personal computer by digitizing the traces and processing the trace position data to obtain instantaneous velocity profiles in the liquid phase surrounding the Taylor Bubble.

2.2. Drag force measurements

When the motion of a trailing Taylor Bubble accelerating behind another Taylor Bubble is observed, the accelerating bubble shows significant deformation of the nose shape and lateral motion from one side of the tube to the other. Under steady flow conditions, a key factor affecting the rise velocity of a Taylor Bubble is the drag force. If the drag force experienced by the Taylor Bubble is reduced as it moves off the tube axis or the shape of the nose becomes asymmetric, the Taylor Bubble could rise faster. In order to determine this, a second experiment has been conducted to directly measure the drag force on a bullet-shaped solid object simulating a Taylor Bubble.

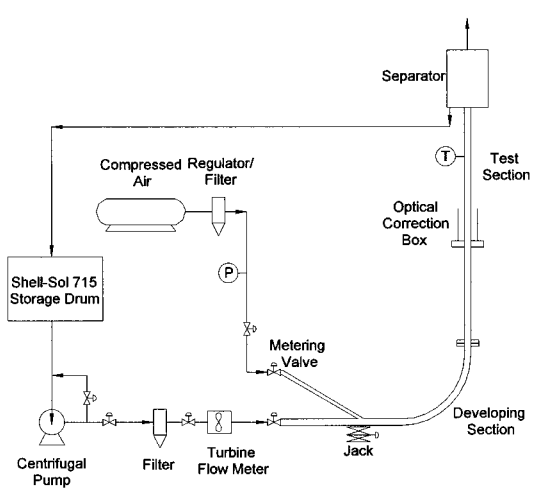

Fig. 1. Experimental setup for the velocity profile measurements.

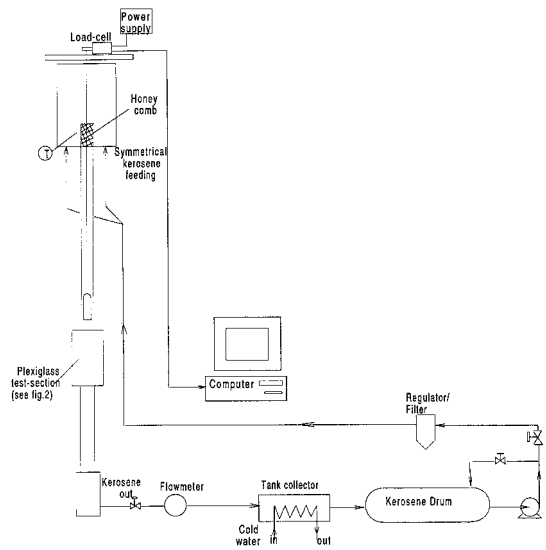

Fig. 2. Test loop for drag force measurement

As shown in Fig. 2, a solid Taylor Bubble was suspended from a load cell and placed in a liquid stream flowing downward in a vertical tube. The lateral position of the bubble could be adjusted using a traversing mechanism as shown in Fig. 3. The diameter of the Taylor Bubble at the tail was 2.0 mm less than the tube inner diameter, so that when the bubble is located at the tube axis, the liquid film would be 1.0 mm thick on all sides. The solid bubble would then be traversed from the tube center towards the left and right walls to measure any change in the drag force. Although the liquid velocity profile ahead of the Taylor Bubble in this experiment is not the same as those encountered in cocurrent upward slug flow, the effect of Taylor Bubble displacement off the tube axis on drag force is expected to be nearly the same since the liquid film starts to fall down at the bubble nose even in cocurrent upward slug flow.

3. Numerical simulation

An extended version of the RIPPLE solution algorithm (Kothe et al., 1991) involving the Volume-of-Fluid (VOF) interface tracking method was used to simulate the hydrodynamics of a Taylor Bubble rising through a stagnant liquid in a vertical pipe. The transient two-dimensional Navier–Stokes equations for an incompressible fluid are given by the following equations,

$$\frac{1}{r}\frac{\partial ur}{\partial r}+\frac{\partial v}{\partial y}=0 \tag{2}$$

$$\frac{\partial u}{\partial t}+\frac{\partial (uu)}{\partial r}+\frac{\partial (uv)}{\partial y}=-\frac{1}{\rho}\frac{\partial P}{\partial r}+\frac{1}{\rho}\left(\frac{1}{r}\frac{\partial}{\partial r}(r\tau_{rr})+\frac{\partial \tau_{yr}}{\partial y}\right)+g_r \tag{3}$$

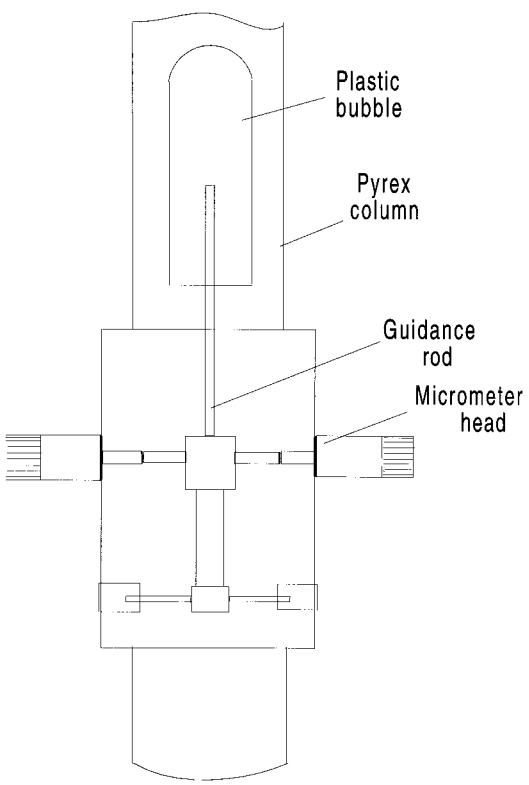

Fig. 3. Solid bubble traversing mechanism

$$\frac{\partial v}{\partial t}+\frac{\partial (uv)}{\partial y}+\frac{\partial (vv)}{\partial y}=-\frac{1}{\rho}\frac{\partial P}{\partial y}+\frac{1}{\rho}\left(\frac{1}{r}\frac{\partial}{\partial r}(r\tau_{ry})+\frac{\partial \tau_{yy}}{\partial y}\right)+g_y \tag{4}$$

where u and v are the radial and axial components of the velocity field respectively, P is the scalar pressure, g is the gravitational acceleration, and τ_{rr}, τ_{ry}, τ_{yr}, τ_{yy} are the components of the Newtonian stress tensor.

RIPPLE uses a finite difference approximation to the Navier–Stokes equations on a cylindrical mesh. These are based on the Taylor series expansion of flow variables that are second order accurate in space and first order accurate in time. A two-step projection technique is employed for the solution of the governing equations. This procedure has the advantage of decoupling the pressure iteration, which is aided by an incomplete Cholesky conjugate gradient (ICCG) solution method, from the momentum equation calculations. The fluid interface is tracked using the VOF method (Hirt and Nichols, 1981), but the surface tension is modeled as a volume force as opposed to the customary explicit boundary condition as explained below.

The free surfaces are reconstructed by means of a scalar VOF function, $F(r, y, t)$,

$$F(r,y,t)=\begin{cases}1, & \text{in the fluid;}\\ >0,<1, & \text{at the free surface cell;}\\ 0, & \text{in the void or secondary fluid.}\end{cases} \tag{5}$$

which is determined by solving a transport equation,

$$\frac{DF}{Dt}=\frac{\partial F}{\partial t}+\frac{u}{r}\frac{\partial (rF)}{\partial r}+v\frac{\partial F}{\partial y}=0 \tag{6}$$

where $F(r, y, t)$ at time $t=0$ is represented, in part, by a shape function, $\eta(r)$.

In RIPPLE, the viscous effects are neglected at the interface and the surface tension coefficient, σ, is assumed to be constant. The pressure at the fluid boundary with curvature, k, is then given by,

$$P_l - P_g = \sigma\kappa \tag{7}$$

which is Laplace's formula for the surface pressure. Since no boundary condition on interface slip is specified in the VOF method, the interface velocity is not directly calculated, but rather determined from interpolation of neighboring velocities. Consequently, the jump condition at the interface is not exactly satisfied. However, this is not overly restrictive because in general the surface tension forces overwhelm the viscous forces. For a bubbly flow, an order of magnitude analysis (Bugg, 1991) revealed that viscous forces are negligible.

In contrast to previous implementations of Eq. (7) as an interface boundary condition, the RIPPLE representation of surface pressure is instead a volume force specified with the continuum surface force (CSF) model (Brackbill et al., 1992). In the CSF model, the surface tension force is recast as a volume force, F_{SV}, non-zero only within free surfaces and is given by,

$$\vec{F}_{sv}(r, y) = \sigma\kappa(r, y)\nabla F(r, y)g(r, y) \tag{8}$$

where the function *g(r, y)* is one of two functional forms,

$$g(r, y) = 1 \quad \text{or} \quad F(r, y)/\langle F \rangle \tag{9}$$

with $\langle F \rangle = 0.5$ being the average of the VOF function. Surface tension forces at the interfaces are thus modelled as a body force in the dynamic momentum equations. The CSF model allows for a more accurate discrete representation of surface tension without the topological restrictions, and leads to surface tension forces that induce a minimum in the free surface energy configuration (Brackbill et al., 1992).

Since the original RIPPLE code was an experimental code, many corrections had to be made including misplaced boundary condition statements, incorrect initialization of conic functions for free surface generation, and conflicting implementation of vector free surface force in ghost cells. Additional modifications of the code by one of the present authors include incorporation of an isentropic model for Taylor Bubble pressure, and a new method for updating VOF values, where the *r* advection for the entire domain is completed before commencing the *y* advection calculation (Bugg, 1991) and directionally altered for each direction at the end of a cycle.

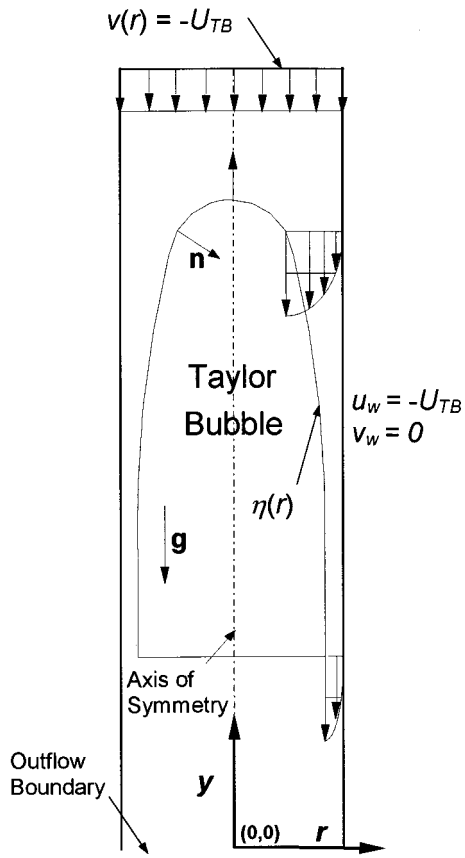

Fig. 4. Taylor bubble simulation configuration: frame of reference moving with Taylor Bubble.

The flow configuration investigated by numerical simulation is shown in Fig. 4. A 6 cm length Taylor Bubble is rising in a vertical tube of 25.6 mm diameter, through a stagnant liquid of density equal to 187.1 kg m^{-3}, under the gravitational acceleration of 9.81 m s^{-1}. The flow was simulated in a frame of reference moving with the Taylor Bubble, so that the liquid and the tube wall move downward. The flow configuration shown in Fig. 4 was solved only for the liquid phase by neglecting the momentum contribution of the gas phase. This approach is reasonable because the pressure variations in the gas phase

are much smaller than those in the liquid and the frictional stresses are likewise smaller in the gas. Thus, the Taylor Bubble may be characterized by the internal, uniform pressure (Akagawa and Sakaguchi, 1966). The governing equations are solved with appropriate boundary conditions: a specified downward inflow condition for the top inlet cross-section, vanishing derivatives of the velocity components (i.e. no change in the axial direction) at the bottom boundary, radial symmetry at the tube axis, and a no-slip condition at the moving rigid wall.

Details of the numerical solution procedure used in the RIPPLE code are given by Kothe et al. (1991). The computational domain measured 20.72 cm in axial direction and 1.28 cm in width. The computational mesh employed and the initial Taylor Bubble shape specified are shown in Fig. 5. Mesh sensitivity studies determined that this grid was the most successful coarse layout used in the computations. The mesh size in the y-direction was uniform at 0.75 mm, and the r-direction mesh was similar in size but expanded slightly away from the pipe wall.

4. Results and discussion

4.1. Velocity field measurements

The rise velocities of the four Taylor Bubble sizes ranging in length from about 3 to 12 cm were nearly constant and agreed well with the theoretical value of 17.54 cm s^{-1} as predicted by Eq. (1). This reflects the fact that the stabilizing entry length for the flow is well below the measuring stations and that the rise velocity is in the inertially-dominated region of flow. The Eötvös number ($E_o = \rho_L D^2 g/\sigma$) was 232 and the Morton number ($M_o = \mu_L^4 g/\rho_L \sigma^3$) was 3.06×10^{-9}.

Fig. 6 shows the near-wall film thickness profile, and hence the Taylor Bubble shape of two 12-cm Taylor Bubbles. The Dumitrescu profile is also plotted for comparison, which is remarkably good, supporting the results of Mao and Dukler (1989). The velocity data obtained from the traces contained the y-component (axial) and r-component (radial). Figs. 7 and 8 show the velocity vector field in the near-wall film region around a 6 cm long bubble, from near the nose to the wake below the tail of the Taylor Bubble. Fig. 9 depicts the two-dimensional flow pattern below the tail of a 6-cm Taylor Bubble far away from the wall region.

Fig. 10 shows the velocity profiles in the falling liquid film around the Taylor Bubble. The film velocity increased from a stagnant condition slightly ahead of the nose to approximately 0.95

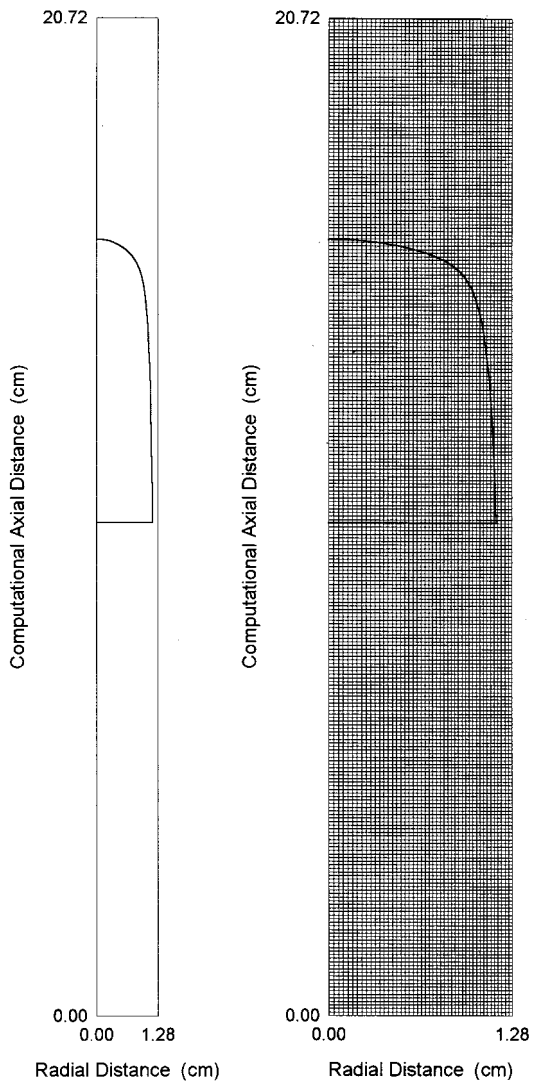

Fig. 5. Computational grid and initial Taylor Bubble shape.

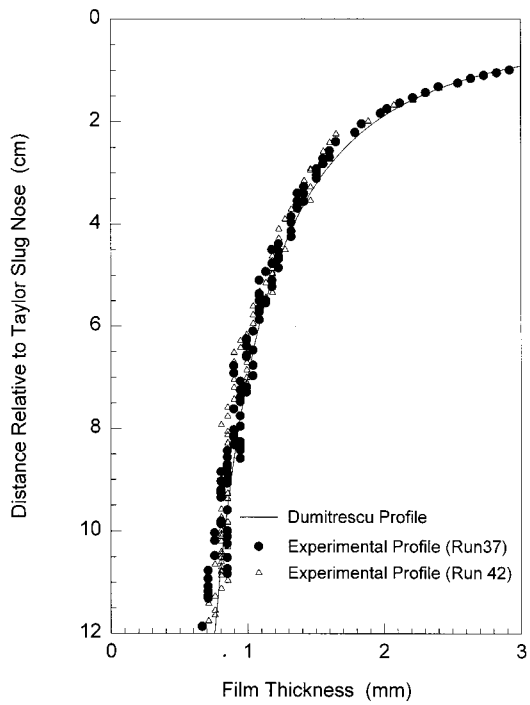

Fig. 6. Shape of Taylor Bubble in film region.

m s^{-1} at the tail. The liquid film accelerated downward and the liquid near the gas–liquid interface moved faster than the liquid near the wall due to negligible shear stress at the interface. On the other hand, as the boundary layer started to develop near the tube wall, the wall shear stress tended to retard the liquid—thus the liquid near the wall accelerated more slowly than the liquid near the interface. The average liquid film velocity at the bubble tail increased from 0.95 m s^{-1} for a 6 cm long bubble to 1.55 m s^{-1} for a 12-cm long bubble.

4.2. Liquid film penetration into wake

Film penetration into the wake slightly away from the wall can be seen in Fig. 11 (Ahmad et al., 1997). Vigorous mixing and circulation of fluid occurred at the tail of the bubble. The velocity of the penetrating film rapidly decays due to this mixing. The Reynolds number of the film at the point of entry into the wake region defined in terms of film thickness, $\mathrm{Re} = 4\delta\rho_L U_f/\mu_L$, was always smaller than 3000 which indicates that the film was laminar for all Taylor Bubbles up to 12 cm in length. The distance to the onset of mixing was identified to be that at which one of the traces in the falling film changed direction near the wall. The film penetration refers to the distance below the tail at which the film ceases its continuous downward motion. Intuitively, since liquid film velocities are greater for longer Taylor Bubbles, we expected the falling film penetration to increase with the Taylor Bubble length. Surprisingly, this was not true. Fig. 12 shows that the film penetrated further for the shorter Taylor Bubbles and was relatively constant for bubbles greater than or equal to 6 cm in length. The mixing took place within approximately less than 1 tube diameter to 1.25 tube diameters, in contrast to Dukler et al. (1985), who speculated that the mixing length is 3–5 times the diameter and gave no dependence on Taylor Bubble length. From

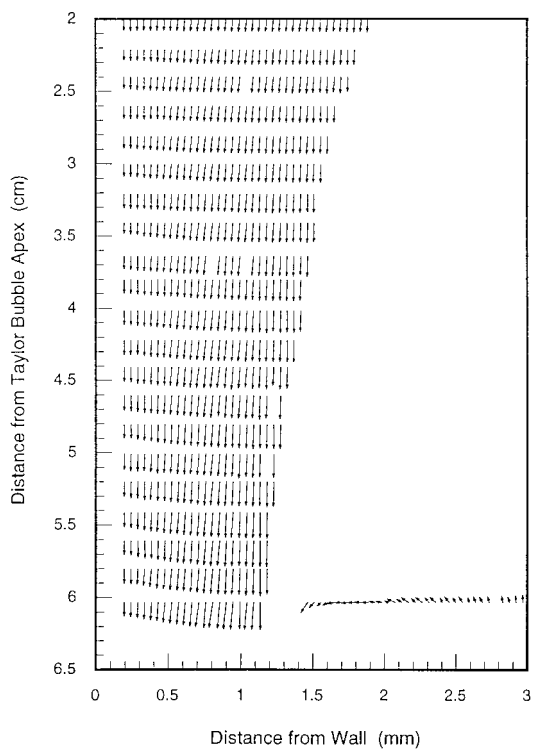

Fig. 7. Velocity vectors in the liquid film region

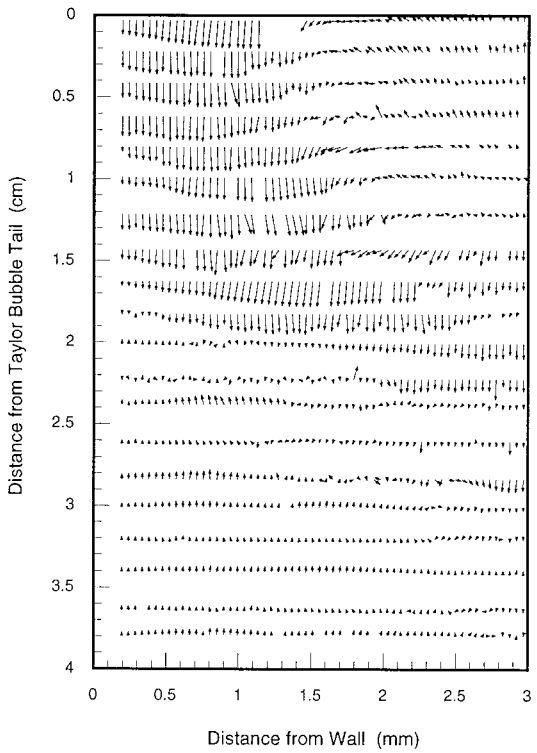

Fig. 8. Near-wall velocity vectors in the wake region

Fig. 12, the film penetration length is accordingly longer than the mixing length—ranging from 1 to 1.5 tube diameters.

It is obvious from observations of the laser dye traces that there is an instability at the shear layer between the core region and the falling liquid film as shown in Fig. 11. In a countercurrent flow of two streams, Kelvin–Helmholtz type instability can readily occur at the boundary and the two fluids would begin mixing for sufficiently large relative velocities. It is also true that the rate of instability growth is greater for larger relative velocities between the two streams (Lamb, 1945). Thus, for longer Taylor Bubbles, the greater liquid film velocity at entry into the wake would give rise to faster growth of instability and could result in shorter penetration distances.

The surprisingly short liquid film penetration in the wake and rapid decay of eddies behind the Taylor Bubble tail suggest that the acceleration of the trailing Taylor bubble is not directly related to the effect of film penetration and large scale eddies in the wake of the leading bubble. Our recent experiments (Hasanein et al., 1996) have indicated that the Taylor Bubble acceleration starts at about 6 diameters below the tail of the leading Taylor Bubble, which is far below the wake. The video pictures of the motion of the accelerating Taylor Bubbles have shown lateral movements and deformed bubble nose shape, which are caused probably by the residual eddies that remain in the liquid flow field following the decay of large scale eddies.

4.3. Comparison of numerical predictions with data

The VOF calculation for low Morton number slug flow with high liquid film velocities was found to be prone to numerical instabilities (DeJesus, 1997). The physical properties of the liquid used in the numerical simulation ($\rho = 187.1$

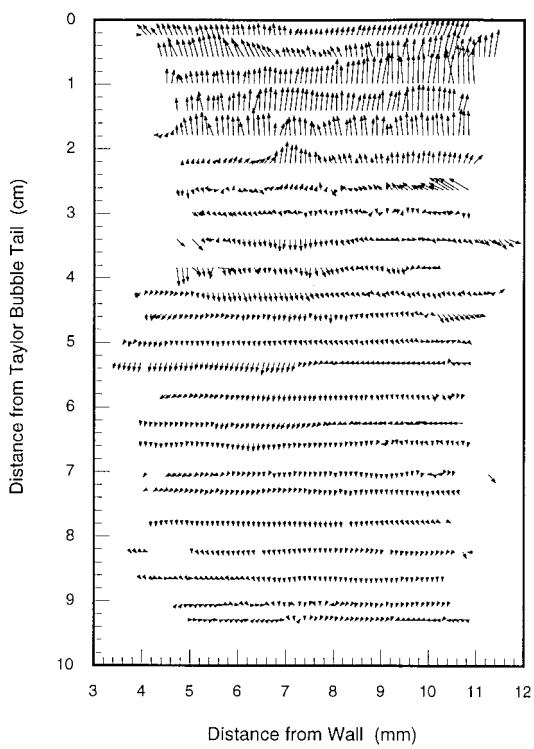

Fig. 9. Flow field in the wake region.

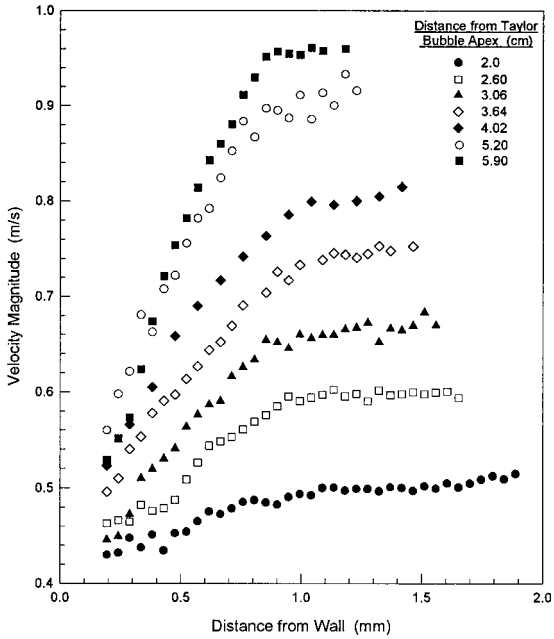

Fig. 10. Velocity profiles in the falling liquid film.

kg m^{-3}, $\mu = 1.4$ mPa s^{-1}, and $\sigma = 6.01$ dynes cm^{-1}) that gave a reasonably stable solution were somewhat different from those used in the experiments ($\rho = 755$ kg m^{-3}, $\mu = 1.43$ mPa-s, and $\sigma = 21.4$ dynes/cm). Although the liquid density

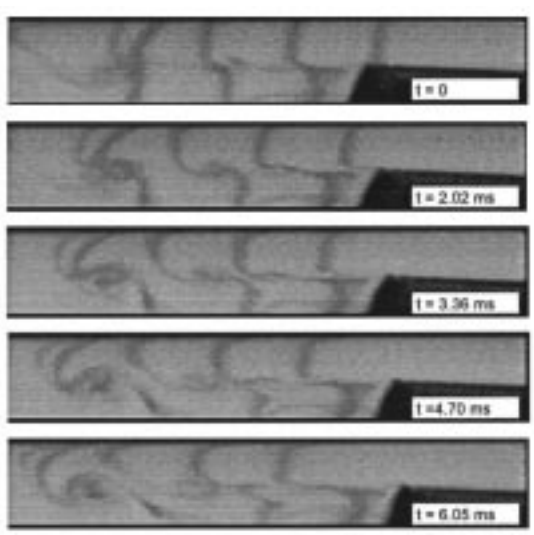

Fig. 11. Liquid film penetration into the wake

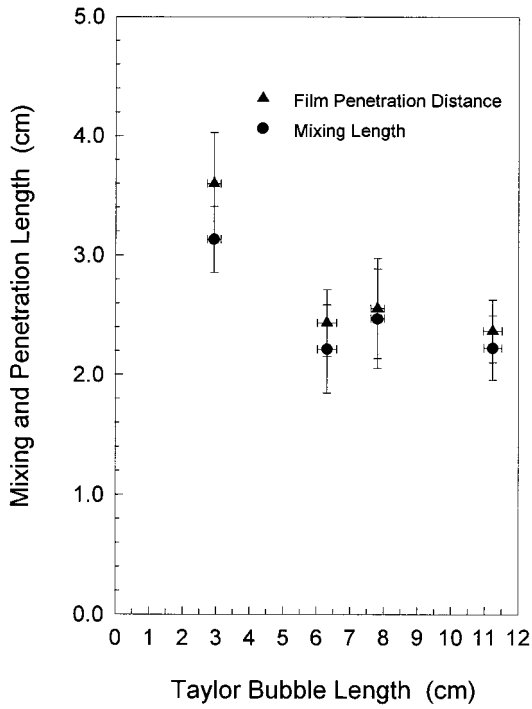

Fig. 12. Onset of mixing and film penetration distances

values were quite different, the rise velocity of a Taylor Bubble in the inertially-controlled region (low Morton number) is independent of the liquid density as evident from Eq. (1).

The predicted Taylor Bubble shape after a simulation time of 0.35 s is in good agreement with the experimental data as shown in Fig. 13. The VOF model predicted shearing off and entrainment of small bubbles at the tail of the Taylor Bubble, while no small bubbles were seen in the experiment. The velocity profiles in the liquid phase predicted by the VOF model are compared with the data in Figs. 14 and 15. The VOF model underpredicted the wall shear stress and velocity profiles near the tube wall, while the differences diminished towards the interface (Fig. 14). The velocity fields predicted for the wake region were similar to those observed experimentally (Fig. 15). The liquid film was predicted to penetrate only about 3 cm below the tail as in the experiments, and eddy motion induced by the film-core interaction was also predicted. However, the complete

decay of eddies required much further distance below the tail probably because of the absence of the turbulence model in the present calculations.

Although the VOF calculation of Taylor Bubbles in inertia-controlled flow regime is still at an early stage and requires improvements to stabilize the calculation and a turbulence model to treat the flow in the wake, the predictions obtained in this work are quite promising for a detailed further study of hydrodynamics.

4.4. Drag force and acceleration of Taylor Bubble

The results of drag force measurement are shown in Figs. 16 and 17 for two liquid flow rates. For a solid Taylor Bubble placed in a downward flow of liquid in a vertical pipe, the radial displacement of the Taylor Bubble from the tube axis clearly results in reduction of the drag force. The measured drag force was not axially symmetric because of the slight misalignment of the bubble axis with respect to the tube wall. However, the present data clearly indicate a reduction in the drag force and therefore an increase in the rise velocity due to any lateral displacement of the Taylor Bubble. Although there are other factors that could contribute to acceleration such as the deformation of the bubble nose, it is conjectured that the residual eddies far below the wake of the leading bubble cause perturbations in the pressure and liquid flow field that in turn cause the trailing bubble to move laterally or deform its shape which can lead to reduced drag force and an increase in the rise velocity.

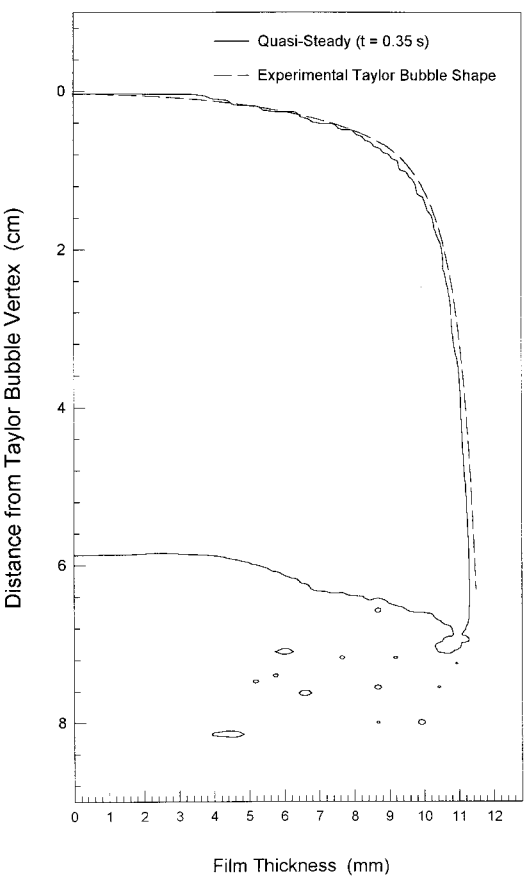

Fig. 13. VOF prediction of the Taylor Bubble shape.

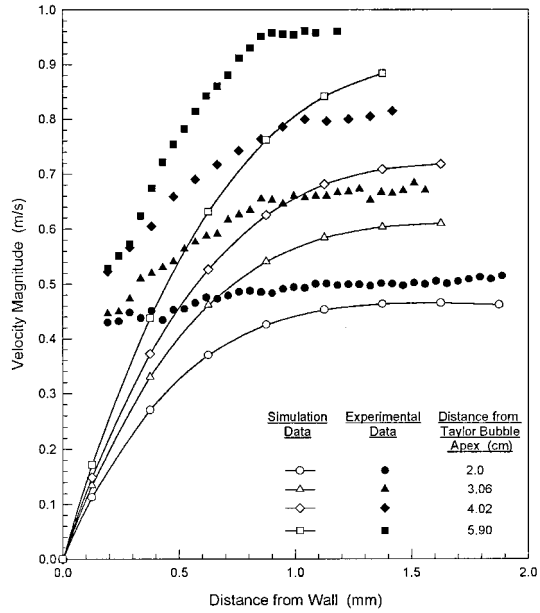

Fig. 14. Comparison of predicted and measured velocity profiles.

5. Conclusions

The photochromic dye activation technique was successfully used in conjunction with a digital high speed video camera and image analysis to

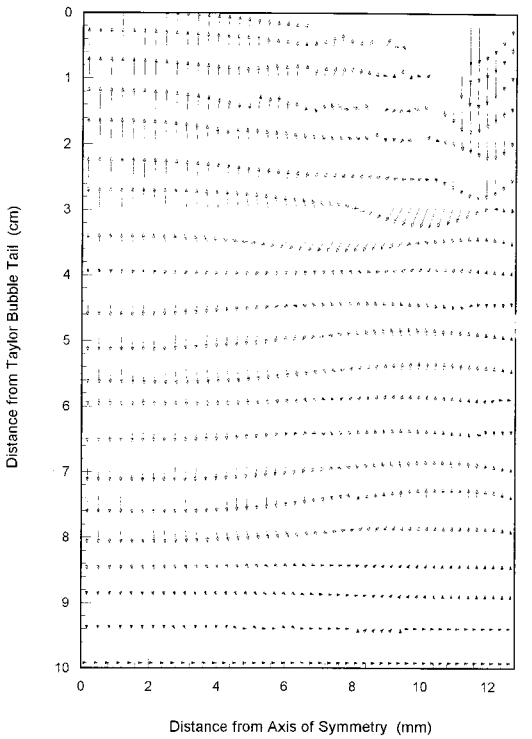

Fig. 15. VOF prediction of velocity fields in the wake.

study the hydrodynamics of a Taylor Bubble rising through a stagnant liquid in a vertical 25.6 mm I.D. tube. A transient, two-dimensional flow model employing the VOF technique to track the position of the gas–liquid interface was also used

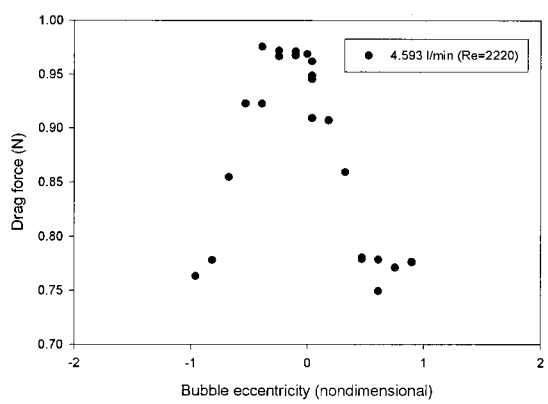

Fig. 16. Drag force variation with radial displacement for a solid Taylor Bubble (Liquid Reynolds No. = 2220).

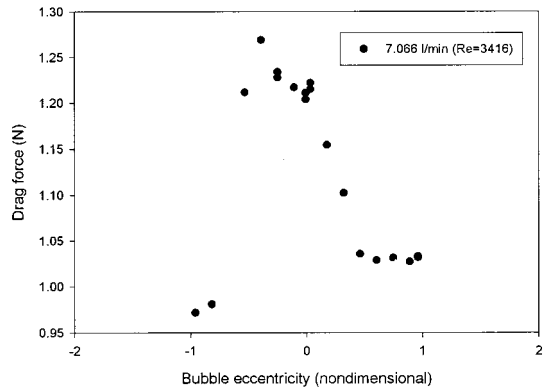

Fig. 17. Drag force variation with radial displacement for a solid Taylor Bubble (Liquid Reynolds No. = 3416).

to simulate the hydrodynamics observed in the experiments. Although more work needs to be performed to improve the stability and incorporate a model of turbulence, the present model was found to be capable of predicting the flow phenomena with reasonable accuracy.

Finally, the drag force has been found to decrease as the Taylor Bubble moves laterally, and this is considered to be important for explaining the acceleration and coalescence of Taylor Bubbles in vertical slug flow.

Acknowledgements

The authors would like to thank the Natural Sciences and Engineering Research Council of Canada for supporting this research.

References

Ahmad, W.R., DeJesus, J.M., Kawaji, M., 1997. Falling film hydrodynamics in slug flow, to be published in Chem. Eng. Sci.

Akagawa, K., Sakaguchi, T., 1966. Fluctuation in void ratio in two-phase flow. Bull. JSME 9, 104–120.

Akagawa, K., Hamaguchi, H., Sakaguchi, T., 1970. Trans. JSME (in Japanese) 36, 1535–1542.

Bendiksen, K.H., 1985. On the motion of long bubbles in vertical tubes. Int. J. Multiphase Flow 11, 797–812.

Brackbill, J.U., Kothe, D.B., Zemach, C., 1992. A continuum method for modeling surface tension. J. Comput. Phys. 100, 335–354.

Brown, R.A.S., 1965. The mechanics of large gas bubbles in tubes -I. Bubble velocities in stagnant liquids. Can. J. Chem. Eng. 43, 217–223.

Bugg, J.D., 1991. An investigation of large bubble dynamics. Ph.D. Thesis, Dept. Mech. Eng., University of Calgary.

Collins, R., DeMoraes, F.F., Davidson, J.F., Harrison, D., 1978. The motion of a large gas bubble rising through liquid flowing in a tube. J. Fluid Mech. 89, 497–514.

Couët, B., Strumolo, G.S., 1987. The effects of surface tension and tube inclination on a two-dimensional rising bubble. J. Fluid Mech. 187, 1–14.

Davies, R.M., Taylor, G.I., 1950. The mechanics of large bubbles rising through extended liquids and through liquids in tubes. Proc. R. Soc. London Ser. A 200, 375–390.

DeJesus, J.M., Ahmad, W.R., Kawaji, M., 1995. Experimental Study of Flow Structure in Vertical Slug Flow, Advances in Multiphase Flow. Elsevier, Amsterdam, pp. 105–118.

DeJesus, J.M., 1997. An Experimental and Numerical Investigation Into the Hydrodynamics of Gas–Liquid Slug Flow. Ph.D. Thesis, Dept. Chem. Eng., University of Toronto.

Dukler, A.E., Maron, D.M., Brauner, N., 1985. A physical model for predicting minimum stable slug length. Chem. Eng. Sci. 40, 1379–1385.

Dumitrescu, D.T., 1943. Strömung an einer Luftblase in senkrechten Rohr. Z. Angew. Math. Mech. 23, 139–149.

Fabre, J., Liné, A., 1992. Modeling of two-phase slug flow. Annu. Rev. Fluid Mech. 24, 21–46.

Fernandes, R.C., Semiat, R., Dukler, A.E., 1983. Hydrodynamic model for gas-liquid flow in vertical pipes. AIChE J. 29, 981–989.

Fukano, T., Matsumura, K., Kawakami, Y., Sekoguchi, K., 1980. Trans. JSME (in Japanese), pp. 2412–2419.

Hasanein, H.A., Tudose, G.T., Wong, S., Malik, M., Kawaji, M., 1996. Slug flow experiments and computer simulation of slug length distribution in vertical pipes. 31st National Heat Transfer Conf., Houston, Aug. 3–6, pp. 211–219.

Hirt, C.W., Nichols, B.D., 1981. Volume of fluid (VOF) method for the dynamics of free boundaries. J. Comput. Phys. 39, 201–225.

Kawaji, M., Ahmad, W., DeJesus, J.M., Sutharshan, B., Lorencez, C., Ojha, M., 1993. Flow visualization of two-phase flows using photochromic dye activation method. Nucl. Eng. Des. 141, 343–355.

Kothe, D.B., Mjolsness, R.C., Torrey, M.D., 1991. RIPPLE: A computer program for incompressible flows with free surfaces. Los Alamos National Laboratory Report LA-12007-MS.

Lamb, H., Hydrodynamics, 6th ed. Dover, New York, 1945.

Mao, Z.S., Dukler, A.E., 1989. An experimental study of gas-liquid slug flow. Exp. Fluids 8, 169–182.

Mao, Z.S., Dukler, A.E., 1991. The effects of surface tension and tube inclination on a two-dimensional rising bubble. Chem. Eng. Sci. 46, 2055–2064.

Moissis, R., Griffith, P., 1962. Entrance effects in two-phase slug flow. J. Heat Transfer 84, 29–39.

Nickens, H.V., Yannitell, D.W., 1987. The effect of surface tension and viscosity on the rise velocity of a large gas bubble in a closed vertical liquid-filled tube. Int. J. Multiphase Flow 13, 57–69.

Nicklin, D.J., Wilkes, J.O., Davidson, J.F., 1962. Two-phase flow in vertical tubes. Trans. Inst. Chem. Eng. 40, 61–68.

Reinelt, D.A., 1987. The rate at which a long bubble rises in a vertical tube. J. Fluid Mech. 175, 557–565.

Shemer, L., Barnea, D., 1987. Visualization of the instantaneous velocity profiles in gas–liquid slug flow. PhysicoChem. Hydrodynam. 8, 243–253.

Street, J.R., Tek, M.R., 1965. Dynamics of bullet shaped bubbles encountered in vertical gas liquid slug flow. AIChE J. 11, 644–650.

Tomiyama, A., Zun, I., Sou, A., Sakaguchi, T., 1993. Numerical analysis of bubble motion with VOF method. Nucl. Eng. Des. 141, 69–82.

.